Available online at www.sciencedirect.com
SCIENCE DIRECT
Catalysis Today 111 (2006) 343–348
CATALYSIS TODAY
www.elsevier.com/locate/cattod

Time-resolved XAFS study on the supporting process of $Rh_6(CO)_{16}$ cluster on γ-Al_2O_3

Akane Suzuki, Yasuhiro Inada, Masaharu Nomura *

Photon Factory, Institute of Materials Structure Science, High Energy Accelerator Research Organization, Oho, Tsukuba 305-0801, Japan

Available online 6 January 2006

Abstract

The structural change during the supporting process of rhodium cluster [$Rh_6(CO)_{16}$] on Al_2O_3 has been studied by time-resolved energy-dispersive XAFS. With the increase of temperature, the bridging CO desorbs continuously at first and almost completely desorbs until 460 K. However, less than 20% terminal CO desorbs until 420 K. About 60% terminal CO desorbs between 420 and 500 K and remaining terminal CO desorbs above 500 K. The Rh–Rh distance decreases from 0.277 to 0.268 nm suddenly between 470 and 490 K then gradually decreases to 0.264 nm. About a half Rh–O interaction grew at the same temperature as the change of Rh–Rh distance and remaining Rh–O grows up above 490 K. The support of rhodium cluster on alumina is controlled by the desorption of bridging CO and the Rh–Rh distance changes simultaneously.
© 2005 Elsevier B.V. All rights reserved.

Keywords: Time-resolved XAFS measurements by DXAFS; The supporting process of Rh cluster

1. Introduction

Knowledge of the dynamic structural change at active sites is important for understanding the catalytic reactions. Many types of catalysts have been developed in order to realize higher catalytic activity as well as longer catalyst life. In general, mono-metal clusters are not used as catalysts because it is aggregated at the catalytic reaction temperature. On the other hand, when the metal carbonyl cluster is deposited on support surface, it does not aggregate to form large metal particles; this is because of the interaction between the metal cluster and the oxide support surface. Thus, the behavior of $Rh_6(CO)_{16}$ has been investigated extensively, mainly by infrared spectroscopy and X-ray absorption fine structure (XAFS) [1–7]. Extended X-ray absorption fine structure (EXAFS) has been widely used to investigate the structure of non-crystalline materials such as metal complexes/clusters on powder surfaces. The cluster structures before and after the supporting treatment can be clarified by XAFS.

The metal carbonyl cluster is supported on the oxide surface by decarbonylation process and it is used as active catalyst. Although it is important to understand the structural change of the cluster and the interaction between the cluster and the support as a function of decarbonylation temperature during the supporting process, the dynamical supporting process is not studied. This is because it takes more than ten minutes to acquire a XAFS spectrum with the usual set-up since the X-ray energy has to be varied using a step-by-step rotation of the crystal monochromator. Such a long acquisition time is not suitable to study dynamically changing structures on the supporting process. Recently, time-resolved dispersive XAFS technique (DXAFS) has been widely used [8–10]. In these methods, X-rays are polychromatized with a bent crystal and X-rays in the required energy range are monitored simultaneously by a position-sensitive detector. Thus, a XAFS spectrum can be measured within a short period if sufficiently intense X-ray can be obtained. Such intense X-ray can be obtained with the help of a tapered undulator installed in the NW2A beamline of PF-AR (Advanced Ring for pulse X-rays) [11,12]. Time-resolved DXAFS set-up is installed in this beam line as shown in Fig. 1, whose time resolution is typically in the order of milliseconds [9]. We have carried out time-resolved XAFS study in order to clarify how and when the strong interaction is formed between the rhodium and the surface OH groups of alumina during the supporting process of 4 wt% Rh clusters.

* Corresponding author. Fax: +81 29 864 2801.
E-mail address: masaharu.nomura@kek.jp (M. Nomura).

0920-5861/$ – see front matter © 2005 Elsevier B.V. All rights reserved.
doi:10.1016/j.cattod.2005.10.046

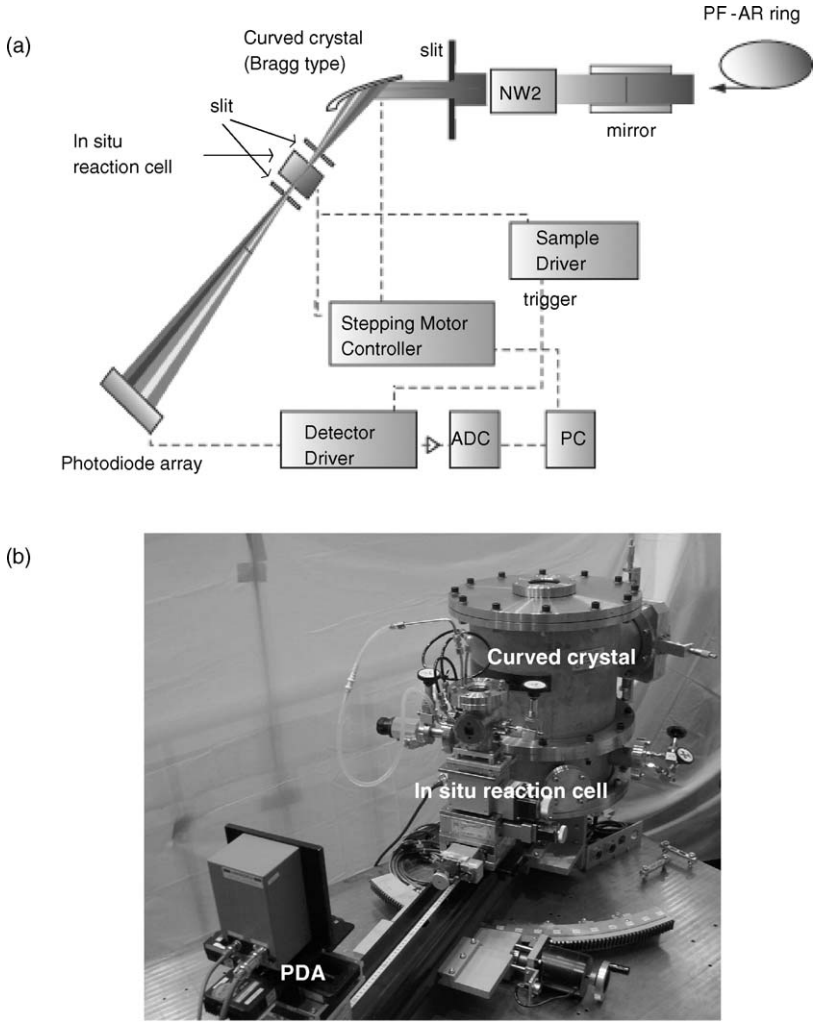

Fig. 1. Schematic diagram (a) and photograph (b) of DXAFS set-up at NW2A. The curved crystal is installed in the chamber filled with helium. The glancing angle of X-ray beam varies continuously across the crystal surface and results in different X-ray energies being reflected from different points on the crystal surface.

2. Experimental

2.1. Sample

$Rh_6(CO)_{16}$ (Aldrich Chemical Co.) was adsorbed on γ-Al_2O_3 by an impregnation method using a hexane or chloroform solution under N_2 atmosphere. γ-Al_2O_3 was pretreated at 773 K for 2 h in dry air prior to using it as the support. The concentration of Rh was 4 wt% as Rh/γ-Al_2O_3. Then the solvent was removed by evacuation.

2.2. In situ reaction cell for DXAFS

This cell was designed to carry out time-resolved DXAFS experiments under catalytic reaction conditions or during the pretreatment of the catalyst. The diffusion of reaction gas into the sample will be limited if a pellet is densely pressed. However, if the pellet is prepared with low pressure, it is easily broken when it is removed from the anvil. Thus, the pellet is prepared by hand pressing the sample powder in a tube (7 mm Ø I.D.) made of stainless steel (SUS 316), then it was mounted in the reaction cell with the tube.

The reaction cell was made of SUS 304 with 120 mL inside volume as shown in Fig. 2. The inside part of the cell is constructed on a flange (H), and the sample is mounted in the cell with the tube used for pellet preparation (A). It can be heated up to 773 K with two cartridge heaters (B) inserted into the cell from outside. Thus, they can be easily changed. The sample temperature is measured with a Chromel–Almel thermocouple and it can be controlled by using a temperature controller (RKC INSTRUMENT INC., RexP48). The chamber (I) seals the reaction environment with an O-ring (G). Kapton® windows seal the cell and transmit the X-ray beam. Kapton windows and the O-ring are water cooled. Gas admission into the cell and evacuation of the gas from it can be remotely controlled from the outside of the experimental hutch.

2.3. DXAFS measurement

Static XAFS measurements were carried out at BL-10B (PF, KEK) with a water-cooled Si(3 1 1) channel-cut monochromator and at NW2A (PF-AR, KEK) using a cryogenically cooled Si(3 1 1) double-crystal monochromator [13]. Fig. 1 shows the schematic diagram of the optics layout of beamline

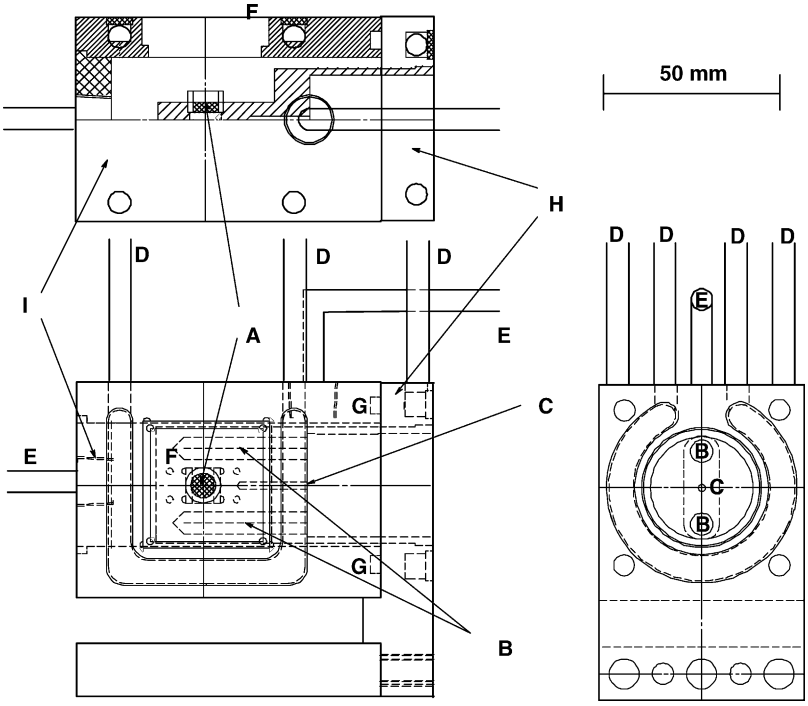

Fig. 2. In situ reaction cell for DXAFS. (A) Sample holder, (B) heater, (C) thermocouple, (D) cooling water pipe, (E) gas inlet, (F) Kapton window, (G) O-ring, (H) cell body and (I) chamber.

NW2A for the DXAFS system. Polychromatic X-rays were obtained by a Si(3 1 1) bent crystal (Bragg-type). The focusing condition for the cylindrically bent crystal is written as Eq. (1) [8].

$$\frac{1}{p}+\frac{1}{q}=\frac{2}{R\sin\theta_{\mathrm{B}}} \tag{1}$$

where p, q, R and θ_{B} are the crystal-to-source distance, the distance between the crystal and the focus point, the radius of the crystal curvature and the Bragg angle at the center of the crystal, respectively. The energy range ΔE is given by Eq. (2).

$$\Delta E = EL\left(\frac{1}{R}-\frac{\sin\theta_{\mathrm{B}}}{p}\right)\cot\theta_{\mathrm{B}} \tag{2}$$

where E, $\Delta\theta$ and L are the X-ray energy at the centre of the crystal and the length of the irradiated crystal, respectively. We measured the DXAFS spectra at the Rh K edge in the energy range of 23–24.2 keV under the conditions of p, q, R, L and θ_{B} being 30 m, 244 mm, 3000 mm, 73 mm and 9.2°, respectively. The horizontal focus size was 1.0 mm. In order to bend the crystal (1 mm thick) into the radius of 3 m, a newly developed water-cooled holder with a fixed curvature was used, in which thermostatted water at 298 K was circulated. A self-scanning photodiode array (PDA, S3904-1024F, Hamamatsu Photonics) coupled with the CsI(Tl)-embrocated fiber optical plate was used as a linear detector. The position of each sensing element was converted into the corresponding X-ray energy by comparing the measured spectrum of a Rh foil with that obtained at BL-10B. DXAFS spectra were measured every 1.6 s (80 ms/exposure × 20 exposures) by changing the sample temperature at a rate of 4 K min^{-1} from 298 to 673 K.

2.4. XAFS analysis

The obtained XAFS spectra were analyzed by using the UWXAFS program [14]. After performing background subtraction using the AUTOBK program [15], the Fourier transformation of the k^3-weighted EXAFS oscillation was obtained, and the structural parameters were determined by a curve fitting procedure in R-space by using the FEFFIT program involving multiple-scattering effects [16].

$$\chi(k)=\sum_j S_0^2 N_j \frac{F_j(k)}{kR_j^2}\sin(2R_jk+\delta_j(k)) \times \exp\left(-2k^2\sigma_j^2-\frac{2R_j}{\lambda_j(k)}\right) \tag{3}$$

where $F_j(k)$ is the backscattering amplitude from each of the N_j scatterers at a distance R_j from the X-ray absorbing atom, $\delta_j(k)$ the central-atom phase shift, σ_j^2 the mean square fluctuation in R_j, $\lambda_j(k)$ the mean free path of the photoelectron and S_0^2 is the overall amplitude reduction factor. The values of $F_j(k)$, $\delta_j(k)$ and $\lambda_j(k)$ were generated by the FEFF 7.0 code for the standard compounds of Rh_2O_3, $Rh_6(CO)_{16}$ and Rh metal. The high-precision static EXAFS data were analyzed by considering all direct and multiple-scattering contributions between 0.08 and 0.6 nm. The time-resolved DXAFS spectra were fitted by using a model function composed of four shells, that is, Rh–CO (terminal carbonyl), Rh–O (oxygen of Al_2O_3 surface) or

Rh–CO (bridge carbonyl) and Rh–CO of carbonyl ligands and Rh–Rh for Rh cluster. In order to reduce the number of independent parameters in the fitting procedure, XAFS spectra of the rhodium cluster were measured at 298, 373, 573 and 673 K with usual manner and the Debye temperatures were calculated from the temperature dependence of the mean square fluctuations. They were used to calculate the mean square fluctuations at a given temperature. The *R*-factors for the fitting were typically 4%.

3. Results and discussion

Fig. 3(a and b) shows a series of DXAFS spectra and their Fourier transforms (FT) at the Rh K edge for $[Rh_6(CO)_{16}]/Al_2O_3$ on the supporting process from 298 to 673 K (4 K min^{-1}). Prior to the decarbonylation of $Rh_6(CO)_{16}/Al_2O_3$, the interatomic distance (*R*) and coordination numbers (CN) are 0.186 ± 0.002 nm and 2.0 ± 0.3 for Rh–C (terminal carbonyl group), 0.225 ± 0.002 nm and 2.1 ± 0.3 for Rh–C (triply bridged carbonyl group), 0.303 ± 0.003 nm and 3.4 ± 0.6 for Rh–CO and 0.277 ± 0.002 nm and 4.4 ± 0.3 for Rh–Rh. These structural parameters are the same as those of $Rh_6(CO)_{16}$ [17,18]. Therefore, it is concluded that $Rh_6(CO)_{16}$ is adsorbed on Al_2O_3 retaining its cluster framework. After the decarbonylation up to 673 K, the *R* and CN of Rh cluster are 0.264 ± 0.002 nm and 5.3 ± 0.3 for Rh–Rh and 0.210 ± 0.002 nm and 1.8 ± 0.3 for Rh–O. These structural parameters also agreed with those obtained by conventional XAFS measurement for $Rh_6(CO)_{16}/Al_2O_3$ [4,18].

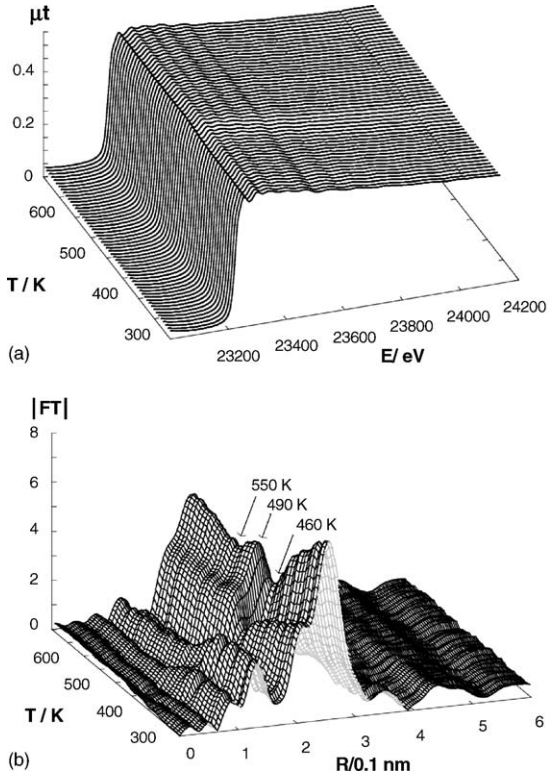

Fig. 3. (a) A series of DXAFS spectra at the Rh K edge and (b) their Fourier transforms at the Rh K edge during the decarbonylation of Rh cluster from 298 to 673 K.

As shown in Fig. 3(a), a prominent change was observed in XANES spectra from 460 to 550 K. In order to estimate the populations of the initial (Rh cluster at 298 K) and the final species (Rh cluster at 673 K after decarbonylation), the observed XANES spectra (23,200–23,400 eV) were tried to reproduce by linear combinations of the reference spectra, as shown in Eq. (4).

$$X_{obs} = C_0X_0 + C_1X_1 \quad (4)$$

where X_{obs} represents an observed X-ray absorption near-edge structure (XANES) spectrum, X_0 and X_1 represent XANES of the initial and the final species and C_0 and C_1 represent their proportions. Fig. 4 shows C_0, C_1 and the residual factor R_f (%) as a function of the decarbonylation temperature. The XANES spectra change drastically between 430 and 490 K and the XANES at 490 K is expressed as the sum of 30% initial and 70% final species. Above 490 K the fraction of two species changes monotonously up to 673 K. However, fairly large residual factor is observed around at 480 K, which indicates that XANES spectra could not be reproduced perfectly by linear combinations of X_0 and X_1 only, suggesting the presence of the third species around 480 K.

Fig. 5 shows typical k^3-weighted EXAFS oscillations for $Rh_6(CO)_{16}/Al_2O_3$ measured by the DXAFS. The quality of the spectra was reasonably good up to 120 nm^{-1} and can be used for the curve fitting analyses. In order to clarify the structural change in detail, k^3-weigted EXAFS functions (χ) were Fourier transformed to obtain the radial structure function.

Fig. 3(b) shows the absolute part of FT ($k^3\chi$) during the decarbonylation process of $Rh_6(CO)_{16}/Al_2O_3$ from 298 to 673 K (4 K min^{-1}). In a series of radial structure functions, three distinct peaks were observed at around 0.18 nm for Rh–C (terminal carbonyl group), 0.21 nm for Rh–O and Rh–C (triply bridged carbonyl group), 0.28–0.30 nm for Rh–Rh and Rh–CO (phase shift uncorrected). The main peak height, which is ascribed to Rh–Rh and Rh–CO interactions, decreases from 320 to 460 K. The intensities of Rh–C(ter.) and Rh–O/Rh–C(br.) decrease simultaneously. However, the main peak height increases above 460 K and the peak ascribed to Rh–O began to increase simultaneously. In order to understand more precisely, we carried out curve fitting analyses of Fourier transforms during the decarbonylation of $Rh_6(CO)_{16}/Al_2O_3$ and the result is shown in Fig. 6 as a function of decarbonylation temperature.

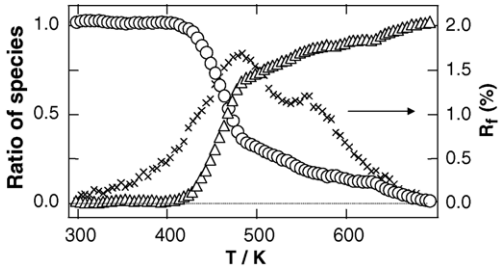

Fig. 4. The proportion of the initial (C_0, ○) and final (C_1, △) species and the residual factor (R_f, ×) derived from XANES as a function of reduction temperature.

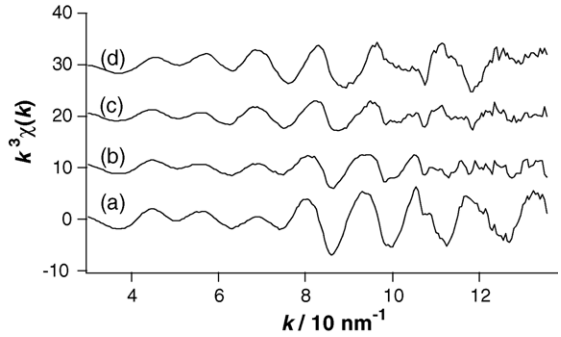

Fig. 5. Typical k^3-weighted EXAFS single measured by the DXAFS for Rh cluster. (a) 298 K, (b) 460 K, (c) 550 K and (d) 673 K.

Regarding the supporting process of the $Rh_6(CO)_{16}$ cluster on Al_2O_3, the time-resolved DXAFS analysis revealed that there were no changes in R(Rh–Rh) parameter between 298 and 460 K. However, the CN of Rh–CO(ter.) decreased from 2 to 1.4 and that of Rh–CO(br.)/Rh–O decreased from 2 to 0.2 between 298 and 460 K. After that, the CN of Rh–CO(ter.) decreased slowly until 600 K. On the other hand, that of Rh–CO(br.)/Rh–O increased between 460 and 490 K. At the same temperature, R(Rh–Rh) decreased monotonously from 0.277 to 0.268 nm, which indicates that Rh cluster shrank. The CN of Rh–CO(br.)/Rh–O and R(Rh–Rh) were almost constant between 490 and 550 K, indicating the existence of a metastable structural state for Rh clusters on Al_2O_3. Above 550 K, the CN of Rh–CO(br.)/Rh–O increased from 1.2 to 2, whereas R of Rh–Rh decreased from 0.268 to 0.264 nm.

Rh–O peak appeared in FT supports the attachment of Rh cluster to the Al_2O_3 surfaces. However, Rh–CO(br.) and Rh–O interactions cannot be separated by XAFS since both interactions give similar interatomic distances. Therefore, we have measured in situ FT-IR spectra under the same temperature programmed conditions with XAFS. At room temperature, twin CO bands were observed at 2080 and

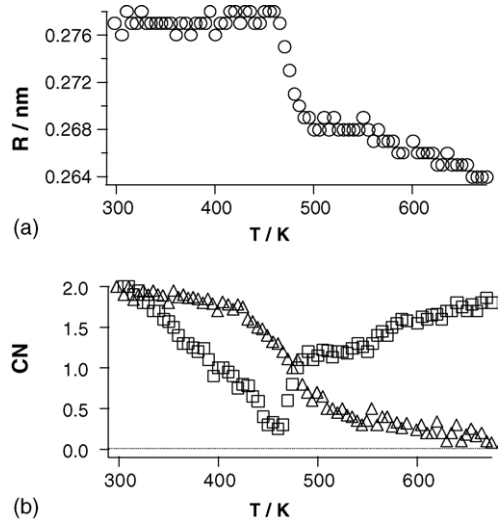

Fig. 6. The bond length (R) of Rh–Rh (○) (a) and the coordination numbers (CN) of Rh–C (terminal) (△) and Rh–C (bridge)/Rh–O (□) (b) determined from XAFS as a function of decarbonylation temperature.

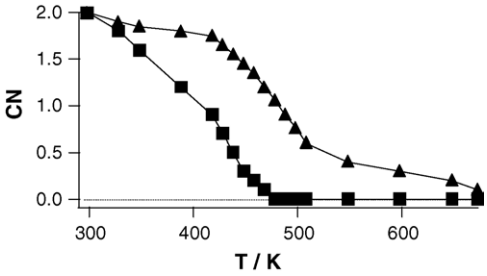

Fig. 7. The coordination number of bridge (■) and terminal (▲) CO on Rh cluster estimated from the peak intensities of FT-IR spectra.

2020 cm^{-1}, corresponding to the symmetric and asymmetric vibration modes of terminal carbonyl groups and a broad band at abut 1800 cm^{-1} assigned to the vibration of bridged carbonyls. Fig. 7 shows the variation of peak intensities ascribed to the terminal and bridge CO as a function of decarbonylation temperature. The change of Rh–C(ter.) agrees with that derived from XAFS, but Rh–C(br.) decreases monotonously. Therefore, the increase of the CN for Rh–CO(br.)/Rh–O above 460 K can be ascribed to the formation of Rh–O bonds with alumina. This indicates that the Rh–Rh bond becomes stronger when the Rh–O interaction is formed on the Al_2O_3 surfaces. The formation of Rh–O bond was supported by the following FT-IR data. When the Rh cluster was treated below 460 K and exposed to CO, it returned to the initial $Rh_6(CO)_{16}/Al_2O_3$, but it did not return to the initial state when treated above 460 K.

Similar temperature programmed decarbonylation experiment was carried out under CO atmosphere of 0.5 atm. In this experiment, the Rh–O peak of $Rh_6(CO)_{16}/Al_2O_3$ is not observed at 460 K and began to appear above 510 K in the XAFS. As written before, Rh–O interaction is observed at 460 K under vacuum. This 50 K discrepancy indicates that the formation of Rh–O bond is controlled by the decarbonylation of bridging CO that makes equilibrium with atmospheric CO.

The structural transformations of rhodium clusters during the supporting process on Al_2O_3 were studied by DXAFS. Bridging CO desorbs until 460 K, which drives the Rh–O bond formation. At the same time the bond length of Rh–Rh decreased. With the increase of temperature, the terminal CO desorbs and the Rh–O interaction with Al_2O_3 surfaces increases.

Acknowledgements

We acknowledge the Photon Factory for provision of synchrotron radiation facilities (2003G294). The present work was partially supported by a Grant-in-Aid for Scientific Research Nos. 16-3780 and 16205005.

References

[1] A.K. Smith, F. Hugues, A. Theolier, J.M. Basset, R. Ugo, G.M. Zanderighi, J.L. Bilhou, V. Bilhou-Bougnol, W.F. Graydon, Inorg. Chem. 18 (1979) 3104.
[2] J.M. Basset, A. Theolier, J. Organomet. Chem. 279 (1985) 147.

[3] G.C. Smith, T.P. Chojnacki, S.R. Dasgupta, K. Iwatate, K.L. Watters, Inorg. Chem. 14 (1975) 1419.
[4] W.A. Weber, B.C. Gates, J. Phys. Chem. B 101 (1997) 10423.
[5] W.A. Weber, B.L. Phillips, B.C. Gates, Chem. Eur. J. 5 (1999) 2899.
[6] B.C. Gates, H.H. Lamb, J. Mol. Catal. 52 (1989) 1.
[7] J.F. Goeliner, B.C. Gates, J. Phys. Chem. B 105 (2001) 3269.
[8] T. Matsushita, R.P. Phizackerley, Jpn. J. Appl. Phys. 20 (1981) 2223.
[9] A. Yamaguchi, T. Shido, Y. Inada, T. Kogure, K. Asakura, M. Nomura, Y. Iwasawa, Catal. Lett. 68 (2000) 139.
[10] A. Suzuki, Y. Inada, A. Yamaguchi, T. Chihara, M. Yuasa, M. Nomura, Y. Iwasawa, Angew. Chem. Int. Ed. 42 (2003) 4795.
[11] S. Yamamoto, K. Tsuchiya, T. Shioya, AIP Conf. Proc. 705 (2004) 235.
[12] T. Mori, M. Nomura, M. Sato, H. Adachi, Y. Uchida, A. Toyoshima, S. Yamamoto, K. Tsuchiya, T. Shioya, H. Kawata, AIP Conf. Proc. 705 (2004) 255.
[13] H. Kawata, T. Mori, H. Adachi, N. Matsugaki, A. Koyama, M. Nomura, AIP Conf. Proc. 705 (2004) 663.
[14] E.A. Stern, M. Newville, B. Ravel, Y. Yacoby, D. Haskel, Physica B 208 (1995) 117.
[15] M. Newville, P. Livins, Y. Yacoby, E.A. Stern, J.J. Rehr, Phys. Rev. B 47 (1993) 14126.
[16] A.L. Ankudinov, B. Ravel, J.J. Rehr, S.D. Conradson, Phys. Rev. B 58 (1998) 7565.
[17] E.R. Corey, L.F. Dahl, W. Beck, J. Am. Chem. Soc. 85 (1963) 1202.
[18] A. Suzuki, M. Nomura, in preparation.